The Observation of the Atomization and Mixing of Doublet-Jets Impinging Sprays at Elevated Ambient Pressures

Tony Yuan*, Cetera Chen, Yu-Da Chen, and Berlin Huang
Department of Aeronautics and Astronautics Engineering, National Cheng Kung University, Tainan, Taiwan, R.O.C.
yahn@mail.ncku.edu.tw and scetera@hotmail.com

Abstract

The atomization and mixing of like-doublet water impinging jets at different ambient pressures (1.0 bar, 6.8 bar and 10.0 bar) and momentum fluxes of the jets were studies in this research. The orifices of the injector (φ=0.3 mm and 0.4 mm) were kept the same and arranged to have impinging angle at +30°/-30°. The momentum flux ratio of the two jets was kept unity. PLIF (Planar Laser Induced Fluorescence) technique and Malvern Spraytec particle size analyzer were adopted to observe the 2-dimensional mass distribution and SMD of the water sprays. In the higher ambient pressure and the larger orifice size experiments, because the jet was less stable, the impinging jets were broken up more uniformly. Besides, the maximum and the local minimum penetration percentage (*P.P.*) occurred at relatively lower momentum fluxes. For the higher aerodynamic instability, the decrease of the mean droplet size of the sprays near the impinging point was also observed at the higher ambient pressure. This study showed that the ambient pressure and orifice size directly influence the disintegration of the impinging jets and the droplet size distributions of the sprays. And the mixing behavior of the impinging jets is closely related to the instability of the liquid jet before impingement.

Introduction

The Doublet liquid jet impinging technique atomizes and mixes the liquids simultaneously that is commonly adopted in the injector design of liquid rocket propulsion systems. It was found that the disintegration of the impinged jets was resulted from the formation of unstable waves caused by the aerodynamic and hydrodynamic instabilities of the liquid flows [1,2]. In cold flow studies, the spray patterns of the impinging jets were characterized into four different modes at increasingly different jet velocities [3]. At fully-developed spray conditions of high jet velocities, liquid atomized immediately after impingement. It also had been shown that the momentum flux or the velocity of the liquid jets as well as the size of the orifices affected the droplet size and mass distributions of impinging sprays. For the doublet impingement of water jets at various momentum fluxes with unity momentum flux ratio, there existed a characteristic momentum flux for the effective breakup of the impinging jets [4,5]. Beyond this characteristic value, the droplets appeared to be uniform distributed in a progressively smaller area. The orifice size mainly influences droplet size and the expansion of the impinging spray, and the study of the effect of the orifice size on impinging jets showed that the impingement of larger jets results in the larger droplets distributing in the wider region [6,7].

In practical, the combustion chamber of the rocket engine is operated in high pressures, such as that hundred pounds thrust level NTO/MMH liquid rocket engines were operated at 6-7 MPa [8-10]. Thus, the impinging jets were disintegrated in the elevated pressure environment during the operation of the rocket engine. In situation, the ambient pressure mainly affects the aerodynamic instability of the jets so as to the primary and secondary break up of the liquid [1,2]. From the observation of the breakup phenomena of the liquid, the higher ambient pressure increased the aerodynamic instability and causes the decrease of the breakup length of the liquid sheet [11,12]. Mean droplet size of liquids was also observed varying with ambient pressure and the axial distance. In general, an inverse relation between mean droplet size and ambient pressure was obtained [11-13].

For the mixing between the impinging jets, Rupe defined the mixing efficiency [14] and proposed that the kinetic energy density ($\rho v^2 d$) ratio of the jets could be used to justify the optimum mixing condition [15]. The mutual penetration of the droplets from individual jets was also observed to relate to the mixing behavior of impinging sprays. The mixing was characterized by the reflective and transmitive (mutual penetration) motions of the atomized liquids, and was depending on jet's velocity or the momentum flux [16,17]. As the mutual penetration of the droplets of the jets approaches 50%, impinging jets achieve the optimum mixing [17]. The like-doublet impingements of larger jets at higher ambient pressure were observed to have a better mixing efficiency for their less mutual penetration [6,18].

It is obvious that atomization and mixing of the propellants is crucial for the performance of liquid rocket engines. Factors such as orifice size, jet velocity, and ambient pressure alter the mass and local mixture ratio dis-

tribution as well as local temperature distribution significantly [18,19]. In this study, the optical observation of the like-doublet water impingement was performed, and the effects of the orifice size, jet's momentum flux, and ambient pressure on the break-up and mixing of the liquid jets were studied.

Experimental Apparatus and Techniques

A nitrogen-compressing flow control system was used to accurately supply the liquid flow in the impinging spray experiments (Figure1). Two turbine-type flow meters (Sponsler, Model: MF20) with an accuracy of 0.25% of the reading were used to real-time monitoring the liquid mass flow rates. The system was carefully calibrated with purified water which was the working fluid in this study. The injector orifices were both 0.4 mm inner diameter (L/d ≈5) and oriented to have a +30/-30 deg impinging angle. The mass flow rate of the jets was varied between 1.0 g/s and 4.5 g/s that corresponded to momentum flux variation between 0.76×10^5 kg/m×s^2 and 12.85×10^5 kg/m×s^2. The momentum flux ratio of the two water jets was kept unity in each experiment.

The spray phenomena of the like-doublet impinging jets were observed in a chamber pressurized by nitrogen at different ambient pressures (1.0 bar, 6.8 bar and 10.0 bar). The pressure chamber was made of stainless steel (∅400 mm×700 mm). Five ∅75 mm quartz windows were mounted on the chamber, four were mounted horizontally to observe the front and side view of the sprays, one window was mounted 30° inclination for CCD observation in PLIF measurements (Figure 2). The chamber pressure was measured by the pressure transducer within ±0.5%.

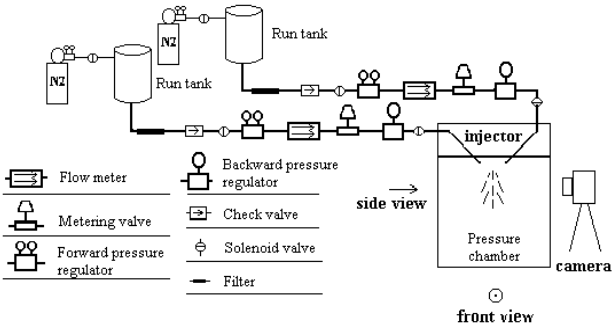

Figure 1 Nitrogen-compressing flow control system.

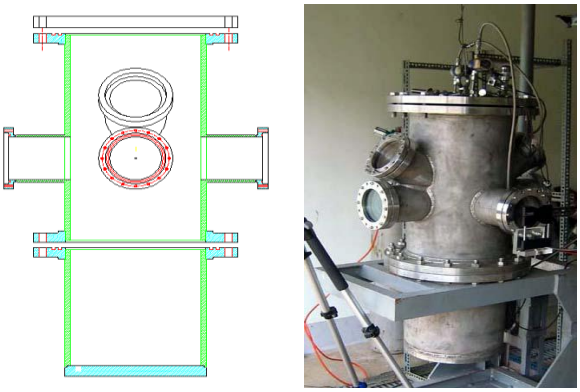

Figure 2 The pressure chamber.

PLIF technique was used to obtain the 2-dimensional mass distribution of liquid spray from either or both jets at 10 mm downstream from the impinging point (Figure 3). A 1 mm×50 mm laser sheet from a second-harmonic Nd-YAG laser (LOTIS, Model: TII) was aligned to cross the spray fan to excite the droplets containing laser dye (Sulforhodamine 101). A 600 nm high-pass filter was used to attenuate the scattered laser light and the fluorescent images of the sprays were acquired by a pseudo-color synchronous CCD camera (1600×1200 pixels). The shutter speed of the camera was set at 110 μsec and the resolution of the image was 0.05 mm. In each experiment, average of 100 fluorescent images was recorded for statistical analysis.

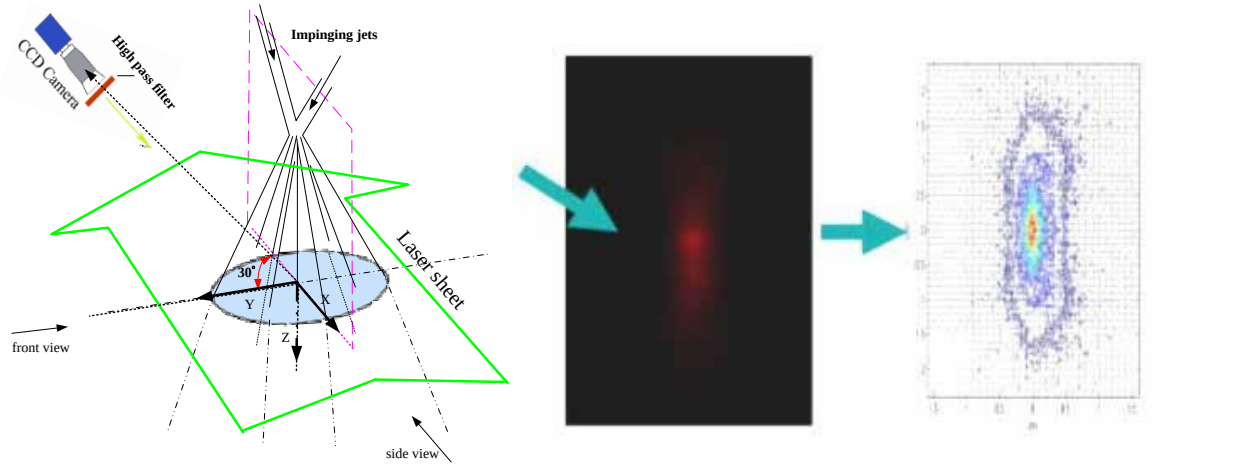

Figure 3 2-D mass probability distribution of the liquid in the PLIF observation.

The local intensities of the fluorescence in the 2-D fluorescent image was directly correlated to the local amount of mass of droplets uniformly containing the excitable dye molecules by

$$f_{x,y} = C_f^{'} I_o(x,y) n_{x,y} = C_f I_o(x,y) m_{x,y} \tag{1}$$

where $C_f^{'}$ is a collective coefficient of the optical setup, spectroscopic characteristics of dye, and temperature and pressure effects on the fluorescent intensities [20]. $I_o(x,y)$ is the local laser intensity, and, $n_{x,y}$ and $m_{x,y}$ are the local number of dye molecules and local mass of the working fluid containing dye, respectively.

Because the dye concentrations were kept invariant in the preparation of all the working fluids, the local fluorescent intensities in the PLIF images was proportional to the local mass [21, 22], and 2-D droplet mass density probability distribution was construct to describe the spray mass distribution. The values of $I_o(x,y)$ were verified to have insignificant difference across the 2-D images, and the local probability density of mass was expressed as

$$P_{x,y} = \frac{m_{x,y}/\Delta x\Delta y}{\int_a^b\int_c^d (m_{x,y}/\Delta x\Delta y)dxdy} \cong \frac{\mathrm{I}_{x,y}/\Delta x\Delta y}{\int_a^b\int_c^d (m_{x,y}/\Delta x\Delta y)dxdy} \tag{2}$$

where (a,b) and (c,d) were the observation ranges in x and y direction, Δx and Δy were the resolution of the observation grid and were both 0.24 mm. For all the contours of 2-D probability density distributions presented in the following, the outer contour of constant probability densities is $3\times10^{-3} mm^{-2}$ and the increment between contours is $9\times10^{-3} mm^{-2}$.

Since the spray of the impinging jets were in the steady state, the local mixture ratios were evaluated by

$$R_{x,y} = \frac{P_{x,y,NTO}\cdot\dot{m}_{NTO}}{P_{x,y,MMH}\cdot\dot{m}_{MMH}} \tag{3}$$

where $\dot{m}$ was the mass flow rate of the test fluid.

The spray patternation index [23] ($P.I.$) and the mixing efficiency [14] (E_m) were also evaluated to express the extend of jet breakup and mixing. $P.I.$ indicates the uniformity of the spray and is zero for the most uniform distribution. $P.I.$ is defined by

$$P.I = \sum_{x,y}\left|\frac{1}{N} - \frac{\dot{P}_{x,y}}{\sum_{x,y}\dot{P}_{x,y}}\right| \times 100 \tag{4}$$

where N is the analyzing pixels covering 8mm×16mm area of the spray image in the present work.

By knowing the local mixture ratios, the mixing efficiency of the spray at the specific plane was calculated by

$$E_m = 100\left[1-\left(\sum_c^d\sum_a^b P_{x,y}\frac{R-r_{sb_{x,y}}}{R} + \sum_{c'}^{d'}\sum_{a'}^{b'} P_{x,y}\frac{R-r_{sa_{x,y}}}{R-1}\right)\right] \tag{5}$$

where R is the global mixture ratio expressed by the mass flow rate ratio of impinging jets. r_{sa} is the local mixture ratio which is larger than R, while r_{sb} is the local mixture which is smaller than R. E_m of 100% indicates the perfect mixing between two liquids.

In addition, penetration percentage ($P.P.$) was also used to indicate the mass percentage of the spray from one impinged jet to cross the center line and penetrate to the other side [17]. It is defined as

$$Penetration\ Percentage = \frac{\left(\sum_c^d\sum_a^0 P_{x,y}\right)_{individual\ jet}}{\left(\sum_c^d\sum_a^b P_{x,y}\right)_{individual\ jet}} \times 100\% \tag{6}$$

For like-doublet jets impinging sprays with the same orifice size and flow momentum rate, $P.P.$ of 50% would ideally result in the optimum mixing efficiency of 100%.

Malvern Spraytec particle size analyzer was used to measure the droplet size at the 10mm downstream centerline region (y=0). Since Malvern measurement gives the SMD as well as their volume percentage distribution of the sizes of the droplets in its line-of-sight probing beam. In conjunction with the mass distribution information provided by PLIF observations, the average droplet sizes of the larger 35% of the total liquid droplets ($SMD_{0.35}$) in different sprays were determined in this study. The details of the estimation procedure of $SMD_{0.35}$ are given in Ref. 24.

Experimental Results

The experimental conditions and results of 0.4 mm water impingements are listed in Table 1 to 3 for different ambient pressures. At atmospheric pressure, the sprays reached their fully-developed condition when the jet momentum fluxes were above 0.76×10^5 kg/m×s^2 (Figure 4). The droplets tended to concentrate near the center line (x=0) of the impinging spray at low momentum flux, by increasing the momentum flux to 3.96×10^5 kg/m×s^2, the ellipse droplets' distribution was observed. The *P.I.* analysis shows *P.I.* of the spray decreased with the increase of the momentum flux (Figure 5), that is, at higher momentum fluxes, the impinging jets broke up more effective and the sprays were more uniformly distributed because of the higher instabilities of jets. In experiments with the ambient pressures at 6.8 bar and 10.0 bar, the *P.I.* of the sprays also decreased with increasing momentum flux (Figure 5), however, the jets were less stable aerodynamically in higher pressure environment, they broke up into more uniform sprays than that of lower ambient pressure conditions as shown by the *P.I.* distributions in Figure 5.

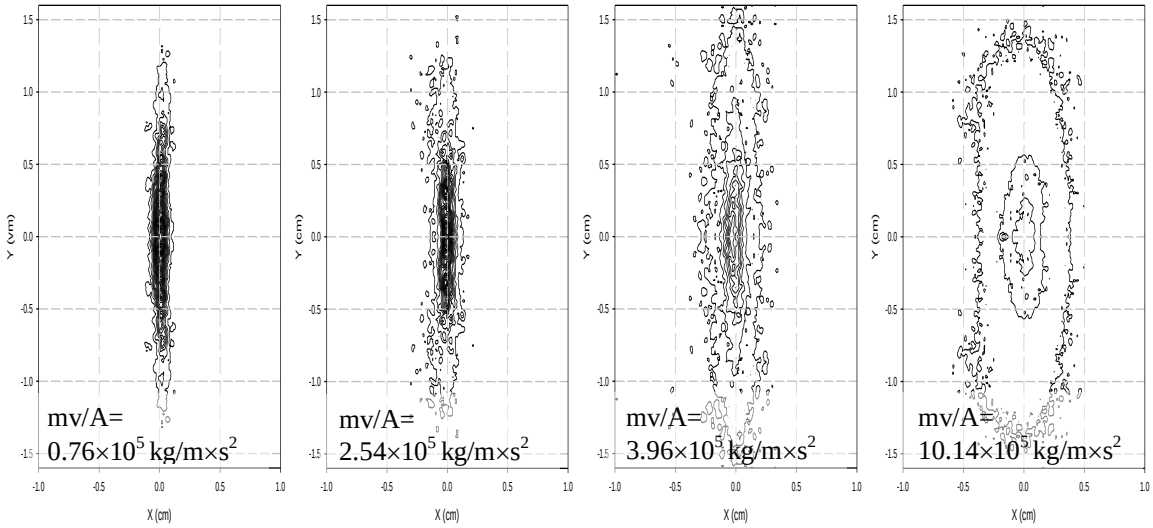

Figure 4 Droplets mass probability density distribution of the water like-doublet impingement. (Orifice diameter: 0.4 mm, ambient pressure: 1.0 bar)

In the mutual penetration behaviors of droplets, the distribution of *P.P.* variations with the momentum flux for fully-developed sprays can be distinguished by three stages (Figure 6): *P.P.* increased with momentum flux to a maximum, *P.P.* rapidly decreased with increasing momentum flux, and then *P.P.* slowly increased with momentum fluxes from a local minimum. At atmospheric pressure, when *P.P.* reached to the local minimum (close to 50%) at a characteristic momentum flux (5.7×10^5 kg/m×s^2), the impinging spray has the best mixing efficiency (≈80%) (Figure 6). The phenomena were similar to the results in previous study [17,25] that was observed and discussed with the impinging jets of 0.3 mm orifice diameter.

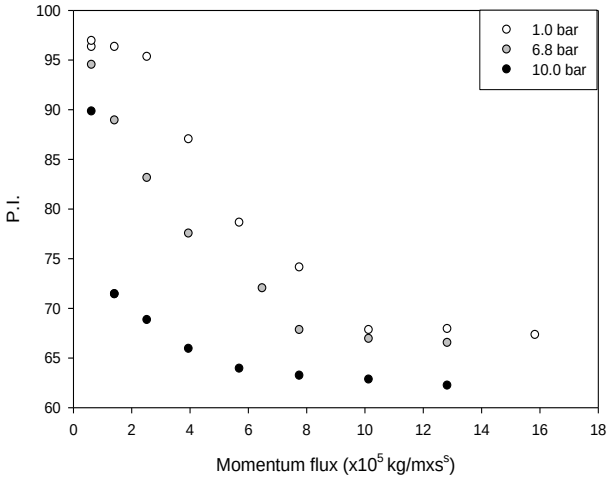

Figure 5 Variations of petternation index (P.I.) with momentum flux for the like-doublet water impinging sprays.

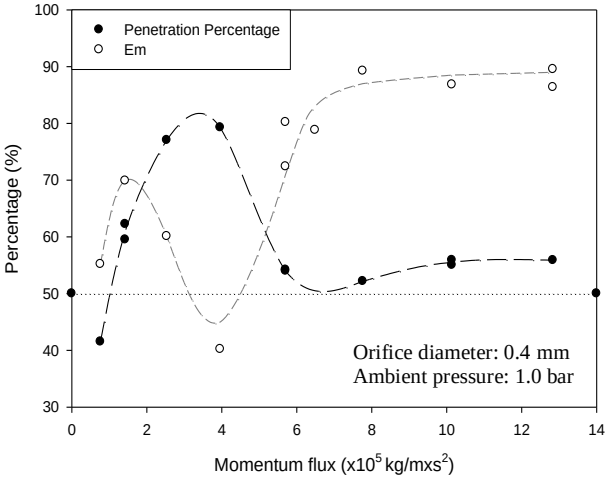

Figure 6 Variations of penetration percentage and mixing efficiency with momentum flux for the like-doublet water impinging sprays.

Table 1 Experimental data of the like-doublet water impingements at the atmospheric ambient pressure

Single jet mass flow rate (g/s)	Jet velocity (m/s)	Jet momentum rate (g×m/s^2)	Jet momentum flux (×10^{5}kg/m×s^2)	Re_D	We	*P.I.*	Penetration (%)	Em (%)
1.1	8.8	9.63	0.76	4016	4360	97	41.5	55.2
1.5	11.9	17.91	1.43	5477	8108	96	59.5	54.1
1.5	11.9	17.91	1.43	5477	8108	-	62.2	69.9
2.0	15.9	31.85	2.54	7303	14414	95	77.0	60.1
2.5	19.9	49.76	3.96	9128	22522	87	79.3	40.2
3.0	23.9	71.66	5.71	10954	32432	78	54.0	72.4
3.0	23.9	71.66	5.71	10954	32432	-	54.2	80.2
3.5	27.9	97.53	7.77	12780	44143	77	52.2	89.2
4.0	31.8	127.39	10.14	14605	57657	68	55.1	78.5
4.0	31.8	127.39	10.14	14605	57657	-	55.9	86.8
4.5	35.8	161.23	12.84	16431	72972	68	55.9	86.4

Table 2 Experimental data of the like-doublet water impingements at the ambient pressure of 6.8 bar

Single jet mass flow rate (g/s)	Jet velocity (m/s)	Jet momentum rate (g×m/s^2)	Jet momentum flux (×10^{5}kg/m×s^2)	Re_D	We	*P.I.*	Penetration (%)	Em (%)
1.0	8.0	7.96	0.63	3651	3604	94	62.2	69.9
1.2	9.6	11.46	0.91	4382	5189	-	41.5	55.2
1.5	11.9	17.91	1.43	5477	8108	90	77.0	60.1
2.0	15.9	31.85	2.54	7303	14414	83	79.3	40.2
2.5	19.9	49.76	3.96	9128	22522	77	59.5	54.1
2.5	19.9	49.76	3.96	9128	22522	-	54.0	72.4
3.0	23.9	71.66	5.71	10954	32432	-	55.9	86.4
3.2	25.5	81.53	6.49	11684	36900	72	54.2	80.2
3.5	27.9	97.53	7.77	12780	44143	68	52.2	89.2
4.0	31.8	127.39	10.14	14605	57657	67	55.1	78.5
4.5	35.8	161.23	12.84	16431	72972	66	55.9	86.8

Table 3 Experimental data of the water like-doublet impingements at the ambient pressure of 10.0 bar

Single jet mass flow rate (g/s)	Jet velocity (m/s)	Jet momentum rate (g×m/s^2)	Jet momentum flux (×10^{5}kg /m×s^2)	Re_D	We	*P.I.*	Penetration (%)	Em (%)
1.0	8.0	7.96	0.63	3651	3604	90	66.0	66.6
1.2	9.6	11.46	0.91	4382	5189	-	40.8	68.4
1.5	11.9	17.91	1.43	5477	8108	71	64.8	70.4
1.5	11.9	17.91	1.43	5477	8108	-	70.0	59.1
2.0	15.9	31.85	2.54	7303	14414	69	53.3	84.8
2.0	15.9	31.85	2.54	7303	14414	-	56.0	87.1
2.5	19.9	49.76	3.96	9128	22522	66	59.8	79.0
3.2	25.5	81.53	6.49	11684	36900	64	60.9	76.6
3.5	27.9	97.53	7.77	12780	44143	63	55.3	88.3
4.0	31.8	127.39	10.14	14605	57657	63	58.5	79.7
4.5	35.8	161.23	12.84	16431	72972	62	56.8	86.2

The *P.P.* variations with the momentum flux at various ambient pressures were qualitatively similar, however, at higher ambient pressures, the maximum *P.P.*, and the local minimum *P.P.* (best mixing efficiency) occurred at relatively lower momentum fluxes (Figure 7). At 6.8 bar, the maximum *P.P.* occurred at the momentum flux of 2.54×10^5 kg/m×s^2 and the best mixing efficiency occurs at the momentum flux of 3.96×10^5 kg/m×s^2, while at 10.0 bar, the maximum *P.P.* occurred at the momentum flux of 1.43×10^5 kg/m×s^2 and the best mixing efficiency occurred at the momentum flux of 2.54×10^5 kg/m×s^2. The results showed that the ambient pressure significantly influenced *P.P.* or the mixing efficiency of the impinging sprays, however the best mixing efficiencies at different ambient pressures were almost the same at about 80% yet occurring at different momentum fluxes.

From the analysis of $SMD_{0.35}$ of impinging sprays at the spray center region 10 mm downstream the impinging point, the result showed that the $SMD_{0.35}$ was almost invariant with the momentum flux of impinging jets at

the atmospheric pressure (Figure 8). However, at higher ambient pressures, the $SMD_{0.35}$ of impinging sprays were significantly reduced at the position of measurement. The reduction of $SMD_{0.35}$ increased with momentum flux and pressure. This indicated that the aerodynamic instability significantly influenced the mean droplet size of the impinging sprays near the impinging point. The higher aerodynamic instability made the size of the larger droplets effectively decreased.

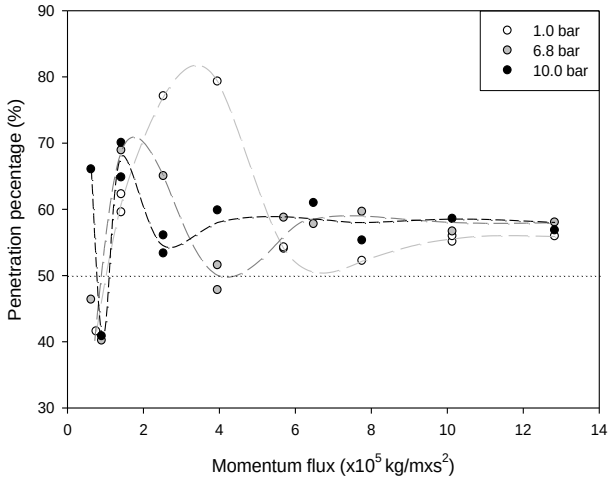

Figure 7 Variations of penetration percentage with momentum flux for the like-doublet water impinging sprays.

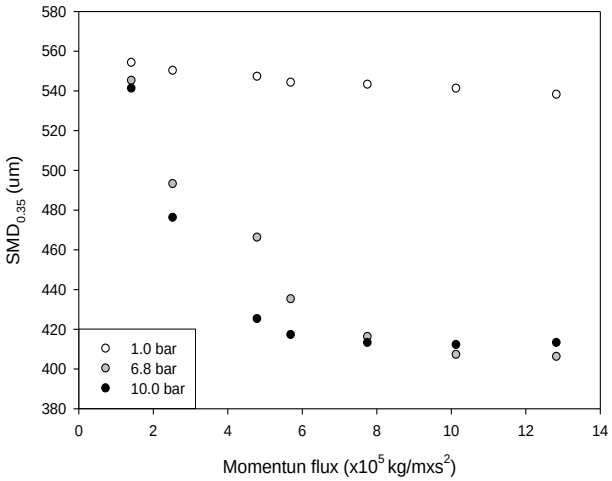

Figure 8 Variations of $SMD_{0.35}$ with momentum flux for the like-doublet water impinging sprays.

In this study, the atomization and mixing of the impinging jets with 0.4 mm orifice diameter are also compared with that of the impinging jets with 0.3 mm orifice diameter [17]. At the same momentum flux, a smaller jet has a lower Reynolds number, thus to a lower hydrodynamic instability. That is, the smaller jets are comparatively stable and more difficult to be effectively atomized than that of the larger jets. Thus, from the analysis of the *P.I.* of the spray, the droplets of the larger impinging jets (φ=0.4 mm) have more uniform distribution than that of the smaller impinging jets (φ=0.3 mm, Figure 9).

The variation of *P.P.* with the momentum flux of the 0.3 mm jet is also qualitatively similar to that of the 0.4 mm jet as is shown in Figure 10. However, the occurrence of the maximum and the local minimum *P.P.* appeared at higher momentum fluxes for 0.3 mm impinging sprays. This also indicated that the mixing behavior of impinging sprays is crucially affected by the instability of the jets.

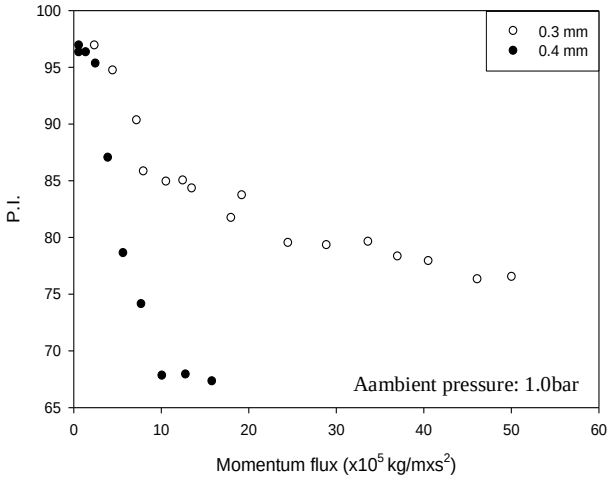

Figure 9 Variations of petternation index (P.I.) with momentum flux for the like-doublet water impinging sprays.

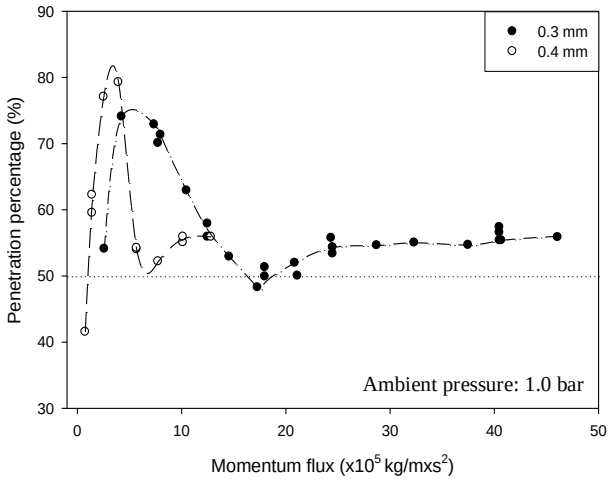

Figure 10 Variations of penetration percentage with momentum flux for the like-doublet water impinging sprays.

Conclusion

This research performed the study of the effect of the ambient pressure and orifice size on the disintegration and mixing of the like-doublet water impinging jets. For higher ambient pressure and larger orifice size, the droplets in the impinging sprays were more uniform distributed due to the increasing instability of the jets before the impingement. Ambient pressure also significantly affected the mean droplet size near the impinging point of the sprays. For sprays in higher ambient pressures, the decrease of the size of the larger droplets was observed. The variation of the *P.P.* with momentum flux is also influenced by the ambient pressure and orifice size. For the higher ambient pressure and the larger orifice size, the maximum *P.P.*, and the best mixing efficiency occur at relatively lower momentum fluxes, which indicated the mixing behavior in impinging sprays is closely related to the instability of the jets before impingement.

References

[1] Dombrowski, N. and Hopper, P. G., *Journal of Fluid Mechanics*, Vol. 18, part 3: 392-400 (1964).
[2] Lefebvre, A. H., *Atomization and Sprays*, Hemisphere Publishing Corporation (1989).
[3] Lai, W. H., Huang, W. and Jiang, T. L., *Atomization and Sprays*, Vol. 9: 277-289 (1999).
[4] Vassallo, P., Ashgriz, N. and Boorady, F. A., *Journal of Propulsion and Power*, Vol. 8, No. 5, Sep-Oct: 980-986 (1992).
[5] Yuan, T., Chen, C., Zhung, Y.-Q. and Huang, B., *Proceedings of the 11th International Symposium on Flow Visualization*, F064, IN, USA, August (2004).
[6] Yuan, T., Chen, C., Huang, B., Yeh, W. and Lin, W., *The 6th Pacific Symposium on Flow Visualization and Image Processing*, 11B-6, Kaohsiung, Taiwan (R.O.C.) (2009).
[7] Lai, W.-H., Huang, W. and Jiang, T.-L., *International Journal of Turbo and Jet Engines*, Vol. 15: 155-164 (1998).
[8] Schindler, R. C. and Schoenman, L., *Journal of Spacecraft and Rocket*, Vol. 13. No. 7, July: 435-442 (1976).
[9] Miyajima, H., Kuroda, Y., Nagashima, R. and Imachi, U., *AIAA-86-1704* (1986).
[10] Schwende, M. A., Munding G. and Schulte, G., AIAA-92-3860 (1992).
[11] Dombrowski, N. and Hopper, P. G., *Chemical Engineering Science*, Vol. 17: 291-305 (1962).
[12] Strakey, P. A. and Talley, D. G., *Proceedings of the 8th International Conference on Liquid Atomization and Spray Systems*, Pasadena, CA, July (2000).
[13] Shen, Y. B. and Poulikakos, D., *Experimental Heat Transfer*, *11*: 23-40 (1998).
[14] Rupe, J. H., Jet Propulsion Lab., *JPL Progress Rept. 20-195*, California Inst. of Technology, Pasadena, CA (1953).
[15] Rupe, J. H., Jet Propulsion Lab., *JPL Progress Rept. 20-209*, California Inst. of Technology, Pasadena, CA (1956).
[16] Ashgriz, N., Brocklehurst, W. and Tally, D., *Journal of Propulsion and Power*, Vol. 17, No. 3, May-June: 736-749 (2001).
[17] Yuan, T., Chen, C. and Huang, B., *Proceedings of the 11th Annual Conference on Liquid Atomization and Spray Systems-Asia*, E2, Taipei, Taiwan (R.O.C.), November (2007).
[18] Yuan, T. and Chen, Y.-D., *Proceedings of the 14th Annual Conference on Liquid Atomization and Spray System-Asia*, Jeju, Korea, October 21~22: 184-190 (2010).
[19] Yuan, T., Chen, C. and Huang, B., *AIAA Journal*, Vol. 44, No. 10: 2259-2266 (2006).
[20] Eckbreth, A. C., *Laser Diagnostics for Combustion Temperature and Species*, Gordon and Breach Publisher (1996).
[21] Talley, D. G., Verdieck, J. F., Lee, S. W., Mcdonell, V. G. and Samuelsen, G. S., *AIAA-96-0469* (1996).
[22] Jung, K., Koh, H. and Yoon, Y., *Measurement Science and Technology*, Vol. 14: 1387-1395 (2003).
[23] Tate, R. W.," *Industrial and Engineering Chemistry*, Vol. 52, No. 10, October: 49A-53A (1960).
[24] Yuan T., and Tsai, B.-Y., *Proceedings of the 23th Annual Conference on Liquid Atomization and Spray System-Americas*, ILASS2011-179, Ventura, CA, USA, May (2011).
[25] Yuan T., and Huang B., *Proceedings of the 23th Annual Conference on Liquid Atomization and Spray System-Americas*, ILASS2011-178, Ventura, CA, USA, May (2011).